Dynamics of a single ion in a perturbed Penning trap: Octupolar perturbation

Martín Lara
Real Observatorio de la Armada, 11110 San Fernando, Spain

J. Pablo Salas[a)]
Area de Física Aplicada, Universidad de La Rioja, 26004 Logroño, Spain

(Received 6 May 2003; accepted 24 May 2004; published online 13 September 2004)

Imperfections in the design or implementation of Penning traps may give rise to electrostatic perturbations that introduce nonlinearities in the dynamics. In this paper we investigate, from the point of view of classical mechanics, the dynamics of a single ion trapped in a Penning trap perturbed by an octupolar perturbation. Because of the axial symmetry of the problem, the system has two degrees of freedom. Hence, this model is ideal to be managed by numerical techniques like continuation of families of periodic orbits and Poincaré surfaces of section. We find that, through the variation of the two parameters controlling the dynamics, several periodic orbits emanate from two fundamental periodic orbits. This process produces important changes (bifurcations) in the phase space structure leading to chaotic behavior. © *2004 American Institute of Physics.*
[DOI: 10.1063/1.1775331]

In this paper we focus on the classical dynamics of a single ion trapped in a perturbed Penning trap. The Penning trap, which is briefly described in the Introduction, is an experimental device which allows physicists to confine charged particles for a long time. Due to imperfections in the design of the experimental setup, some perturbations can be added to the original model. In particular we consider the so-called octupolar perturbation, which is composed by quartic terms. Because of the axial symmetry of the problem, the system has two degrees of freedom. Our objective is to perform an exhaustive numerical study of the nonlinear effects caused by the imperfections on the Penning trap. In this way, through the variation of the parameters controlling the dynamics, we explore the evolution of the phase space structure of the system by the numerical continuation of the families of periodic orbits and surfaces of section. The main result we find is that the presence of the perturbation produces important changes (bifurcations) in the phase space structure leading to chaotic behavior.

I. INTRODUCTION

Classical and semiclassical dynamics has proven to be very useful for interpreting the quantum dynamics of real atomic and molecular systems, even when the classical dynamics is chaotic and the quantum dynamics is strongly mixed.[1] Under these conditions, it is well known that the study of periodic orbits and phase space structure provides useful information that can be compared with the behavior of the corresponding quantum system and with experiments.[1,2] Since the pioneering work of Gutzwiller,[3] a plethora of authors (see, e.g., Ref. 4 and references therein) have tried to state a clear relation between classical periodic orbits and quantum eigenfunctions. In particular, the hydrogen atom in the presence of external fields is one of the most famous systems on which all those theories have been applied and successfully corroborated by experiments. For example, several beautiful photoabsortion experiments on highly excited Rydberg atoms in parallel/crossed magnetic and/or electric fields showed that each oscillation in the spectra can be correlated with a classical periodic orbit.[5,6] Furthermore, periodic orbit bifurcations are visible in the experimental data.[6] In relation to molecular systems, we can cite the H_2O molecule, which has been extensively studied from the classical,[7] semiclassical, and quantal[2] points of view.

Once the importance of the periodic orbits in atomic/molecular systems has been stated, in this paper we continue the preliminary study of Ref. 8. In that paper the phase space structure of a single ion trapped in a realistic perturbed Penning trap is studied for the special case in which the trapped ion's orbital plane rotates with constant angular velocity equal to the Larmor frequency. Now we consider a more general case, and also provide full details in the procedures.

The Penning trap is a widely used device in atomic physics for trapping charged particles.[9–11] Because charged particles can be confined in a Penning trap for a long time, experiments have led, among other things, to very precise spectroscopic measurements,[12] Coulomb crystal studies,[13] and accurate atomic clocks.[14] Moreover, as Cirac and Zoller[15] introduced, one of the most important applications of ion traps today is in quantum computing. For a general review of the state of the art of ion trapping, we refer the reader to Ref. 16.

Besides the above-cited features, Penning traps proved to be a very useful theoretical and experimental tool for studying nonlinear collective phenomena in classical and quantum mechanics (see, e.g., Ref. 17 and references

[a)]Electronic mail: josepablo.salas@dq.unirioja.es

therein). When we are dealing with a perfect Penning trap, the motion of the noninteracting trapped ions remains harmonic. However, as it was studied by several authors,[18–21] electrostatic field perturbations may arise from imperfections in the physical design of the electrodes as well as from misalignments in the experimental mounting. We can separate these perturbations into two groups: harmonic and anharmonic perturbations. In particular, the second group is the most interesting because it leads to nonlinear motion.

Because today's technology allows one to trap a single ion, hence it has sense to consider the theoretical study of the dynamics of a single trapped ion. This possibility was also pointed out by Bergeman for a single cooled atom trapped in a quadrupole magnetostatic trap.[24] As we will see in the next section, a general theoretical study of the motion of a single ion in a perturbed Penning trap is an almost impossible task. Hence, in this paper we only consider axially symmetric perturbations of the three-dimensional Penning trap, which is also axially symmetric. In particular, we will treat the *octupolar* perturbation.

As we remarked in a previous paper,[25] although electrostatic perturbations are usually undesirable, they may be experimentally added by modifying the electrostatics of the trap. Theoretical works along this line were done by Backhaus *et al.*[26] An alternative to these kinds of perturbed traps, based on a combined Penning–Ioffe trap, has been recently suggested.[27]

The paper is organized as follows. Section II is devoted to the posing of the problem. A general model for the nonlinear electrostatic imperfections is assumed. In order to manage a two-degrees-of-freedom system, we assume that only axial-symmetric electrostatic perturbations take place. Moreover, among all the axial-symmetric nonlinear terms appearing in the model, we only consider the axial-symmetric octupolar one. In Sec. III, from a Hamiltonian formulation, we derive the equations of motion and we establish the relevant parameters controlling the dynamics. By studying the effective potential energy surface of the system, we can understand part of the dynamics. In Sec. IV, we study the evolution of the fundamental families of orbits that determine the phase space structure. To do that, we use the numerical continuation of families of periodic orbits and Poincaré surfaces of section. Special attention is paid to two points: the stability of the periodic orbits and their bifurcations. Finally, in Sec. V we summarize the results.

II. PROBLEM

One of the most popular ion traps is the *Penning trap*.[9,19] The Penning trap provides three-dimensional trapping by means of an axially symmetric (''*perfect*'') quadrupole electric field plus a static magnetic field along the z direction. The perfect quadrupole electric potential is achieved by means of a set of three electrodes. These electrodes are infinite hyperboloids of revolution whose equations are

$$\frac{\rho^2}{\rho_0^2}-\frac{z^2}{z_0^2}=\pm 1, \quad \rho^2=x^2+y^2. \tag{1}$$

The minus sign in Eq. (1) stands for the electrode called the *ring*, while the plus sing refers to the other two electrodes called *end-cap* placed above and below the ring. The constants ρ_0 and z_0 are, respectively, the inner radius of the ring electrode and the half distance between the two end-caps. Finally, $\rho_0^2=2z_0^2$. A voltage U_0 is applied to the end-cap electrodes with respect to the ring. Hence, for a single ion of mass m and charge q, the perfect quadrupole electrostatic potential is given by

$$V(x,y,z)=\frac{mw_z^2}{4q}(2z^2-x^2-y^2), \tag{2}$$

where $w_z=\sqrt{4qU_0/(mR_0^2)}$ is a frequency and $R_0^2=\rho_0^2+2z_0^2$. The magnetic field $\mathbf{B}=B\hat{\mathbf{z}}$ introduces the cyclotron frequency $w_c=qB/m$.

The quadrupole potential acts as a trap only in one dimension, along the z axis between the end-cap; while the motion in the radial *xy*-plane is unstable. The presence of the magnetic field along the z axis will provide the complete trapping. In this arrangement, the ion dynamics is harmonic.

A. Electrostatic perturbations

Electrostatic perturbations may arise from imperfections in the physical design of the electrodes as well as from misalignments in the mounting.[19] We model the electrostatic imperfections by means of the multipole expansion of the electrostatic potential.[28] This expansion, in spherical (r,θ,ϕ) coordinates, takes the form

$$V=\sum_{l\geqslant 0} V_l, \quad V_l=\sum_{k=0}^{l} a_{l,k}r^l\mathcal{P}_l^k(\cos\theta)\cos(k\phi), \tag{3}$$

where $\mathcal{P}_l^k$ are the Legendre polynomials with $0\leqslant k\leqslant l$. Note that, while for $l<3$ the motion remains harmonic, higher orders $l\geqslant 3$ will introduce nonlinearities in the motion. In general, most of the terms in Eq. (3) can be made negligible by means of a careful design of the electrodes. For example, in real Penning traps, the electrodes can be assumed to be symmetrical with respect to the *xy*-plane and cylindrical symmetric. Hence, all the terms in Eq. (3) with l odd and $k\neq 0$ vanish and we can write Eq. (3) as

$$V=V_2+U_0\sum_{l\geqslant 2} a_{2l}\left(\frac{r}{R_0}\right)^{2l}\mathcal{P}_{2l}^0(\cos\theta), \tag{4}$$

where we have dropped the constant term V_0 and where V_2 is the perfect quadrupole potential. With this model, the electrostatic perturbations depend on the actual geometry of the trap, because the coefficients a_{2l} describe how far from the ideal configuration are the electrodes. In this work, we consider the contribution of the first term in the expansion (4): the *octupolar* V_4

$$V_4=a_4\frac{U_0}{R_0^4}[8z^4-24(x^2+y^2)z^2+3(x^2+y^2)^2]. \tag{5}$$

The octupolar term is the main perturbation in a real trap where the electrodes are approximated by electrodes of spherical section.[18] Moreover, we can consider the presence

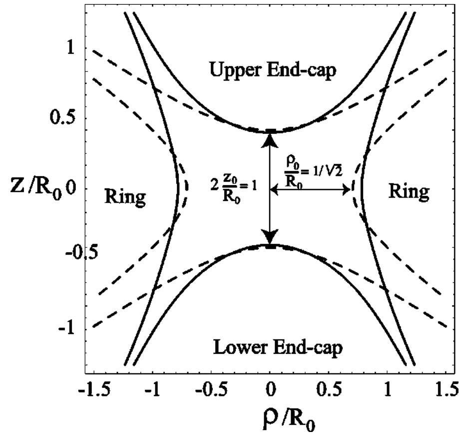

FIG. 1. Experimental realization of the octupolar perturbed Penning trap. The dashed lines correspond to the ideal quadrupole electrode configuration, while solid lines correspond to the octupolar perturbed electrodes for $a=0.1$.

of V_4 not only as an undesirable perturbation, but a term we can intentionally introduce by means of a specific design of the electrodes different from the ideal one. Hence, we can express the complete electrostatic potential $V=V_2+V_4$ as

$$V=\frac{mw_z^2}{4q}\left\{2z^2-(x^2+y^2)+\frac{a}{R_0^2}[8z^4-24(x^2+y^2)z^2+3(x^2+y^2)^2]\right\}, \tag{6}$$

where $a=a_4$. Figure 1 presents a typical configuration of electrodes when a octupolar contribution is added.

III. EQUATIONS OF MOTION

The Hamiltonian defining the motion of a particle of mass m and electrical charge q moving with velocity $\mathbf{v}$ under the action of electromagnetic forces is given by

$$\mathcal{H}=\frac{1}{2}(\mathbf{P}-q\mathbf{A})^2-qV, \tag{7}$$

where V and $\mathbf{A}$ are, respectively, the electrostatic and the magnetic vector potentials. In our case, the electrostatic potential V is from Eq. (6), and the magnetic vector potential is

$$\mathbf{A}=\frac{B}{2}(-y,x,0) \tag{8}$$

for a magnetic field $\mathbf{B}=-B\hat{\mathbf{z}}=\nabla\times\mathbf{A}$. Using cylindrical coordinates $(\rho,z,\phi,P_\rho,P_z,P_\phi)$ we get

$$\mathcal{H}=\frac{1}{2m}(P_\rho^2+P_z^2)-\frac{w_c}{2}P_\phi+\frac{P_\phi^2}{2m\rho^2}+\frac{m}{8}(w_c^2-2w_z^2)\rho^2+\frac{m}{2}w_z^2z^2+\frac{a}{4R_0^2}(8z^4-24\rho^2z^2+3\rho^4). \tag{9}$$

Because the polar angle ϕ is cyclic, the z-component of the canonical angular momentum P_ϕ is an integral. At a first glance, Eq. (9) depends on the parameters (m,w_c,w_z,a,P_ϕ,R_0). However, it is possible to reduce the number of the parameters by means of the following procedure. First, we define the dimensionless time $\tau=w_ct$ and the dimensionless coordinates $\rho'=\rho/R_0$, $z'=z/R_0$. After applying these transformations to Eq. (9) and after dropping primes in variables to simplify the notation, we get the dimensionless Hamiltonian

$$\mathcal{H}=\frac{1}{2}(P_\rho^2+P_z^2)+U(\rho,z), \tag{10}$$

being $U(\rho,z)$ the effective potential

$$U(\rho,z)=-\frac{P_\phi}{2}+\frac{P_\phi^2}{2\rho^2}+\frac{1}{8}(1-2\delta^2)\rho^2+\frac{1}{2}\delta^2z^2+\frac{1}{4}a\delta^2(8z^4-24\rho^2z^2+3\rho^4), \tag{11}$$

and where we have defined $\delta=w_z/w_c$. After this transformation, the parameters appearing in Eq. (10) reduce to δ, a, and P_ϕ. Note that the octupolar term is controlled by two dimensionless parameters. On the one side by a, that indicates the physical deformation of the electrodes, and on the other by δ which modulates the effect of the deformation and determines the ratio between the axial and the cyclotron frequencies, e.g., the ratio between the electrostatic and the magnetic interactions.

The Hamiltonian equations of the motion arising from Eq. (10) are

$$\begin{aligned}
\dot{\rho}&=P_\rho,\\
\dot{P}_\rho&=\frac{P_\phi^2}{\rho^3}-\frac{1}{4}(1-2\delta^2)\rho-a\delta^2(3\rho^3-12\rho z^2),\\
\dot{z}&=P_z,\\
\dot{P}_z&=-\delta^2z[1+4a(2z^2-3\rho^2)],
\end{aligned} \tag{12}$$

being the (ρ,z)-motion decoupled from the angular motion

$$\phi=\phi_0-\frac{1}{2}t+P_\phi\int\frac{dt}{\rho(t)^2}. \tag{13}$$

For the particular case $a=0$, system (12) recover the unperturbed motion of the trapped ion: While motion in the z direction is always oscillatory, the trapping condition

$$\delta<1/\sqrt{2},\quad \text{i.e.,}\quad w_z/w_c<1/\sqrt{2} \tag{14}$$

applies for confined (unperturbed) motion in the ρ direction.[21]

At this point, it is necesary to note that similar (quartic) potentials like Eq. (6) have been widely used in celestial mechanics to study the orbital dynamics of axisymmetric stellar systems.[22,23]

A. Potential energy surface

In order to know how the perturbations modify the perfect trapping, it is useful to study the shape of the effective potential U as the parameters (P_ϕ,δ,a) vary.

For $P_\phi=0$, the centrifugal barrier does not exist, and the motion takes place on a vertical $(\xi=\pm\rho,z)$-plane—where we use ξ instead of ρ in order to consider negative values—

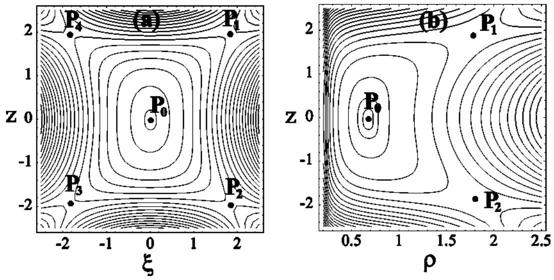

FIG. 2. (a) Equipotential curves of $U(\xi,z)$ for $P_\phi=0$. (b) Equipotential curves of $U(\rho,z)$ for $P_\phi=0.2$. All figures for $a=0.1$ and $\delta=0.25$. Dimensionless units are used.

that rotates with constant angular velocity $-1/2$, e.g., $-w_c/2$. In this rotating plane, $U(\xi,z)$ shows five critical points [see Fig. 2(a)]

A minimum $P_0=(0,0)$, and four symmetrically located saddle points $P_{1,2,3,4}$ at

$$P_{1,2,3,4}=\frac{1}{2\delta}\left(\pm\sqrt{\frac{1+4\delta^2}{15a}},\pm\sqrt{\frac{1-\delta^2}{10a}}\right). \tag{15}$$

Hence, the effect of the octupolar perturbation is to create four equivalent channels of escape through which the ion is able to leave the trap. Remark that the saddle points are equilibria with respect to the rotating frame and circular trajectories with constant angular velocity $-1/2$ in the inertial frame of the trap.

The energies of the critical points are

$$E_0=0, \quad E_S=E_{1,2,3,4}=\frac{1+8\delta^2-14\delta^4}{960\delta^2 a}. \tag{16}$$

When δ increases the energy E_S decreases with the limit

$$\delta^2=\frac{2+\sqrt{15/2}}{7}, \quad \Rightarrow \quad \delta\approx 0.823$$

where $E_S=E_0=0$.

For $P_\phi\neq 0$, the ion cannot pass through the center of the trap, because of the centrifugal barrier. Now, the effective potential also presents a minimum P_0 located at the axis ρ and two symmetrical saddle points P_1 and P_2 [see Fig. 2(b)]. However, although the analytic expressions of these points can be obtained analytically by means of the algebraic expression of the roots of a third degree polynomial, these solutions are cumbersome and do not shed much light on the influence of the parameters a and δ. In this way, we have computed them numerically finding a similar behavior to the case $P_\phi=0$. We also found similar behavior if approximate analytic solutions are used. These approximate solutions are easy to finding by a usual series expansion method.

As a general conclusion, we can cure the effect of the octupolar perturbation by working with cyclotron frequency w_c much bigger than the w_z frequency, e.g., $\delta\ll\delta_\ell$. We remark that this situation corresponds to the usual experimental conditions.[29–32]

IV. PHASE SPACE STRUCTURE

The phase space structure is mainly characterized by the number of the periodic orbits living in phase space, and by their stability. Once a periodic orbit is computed, the stability of that orbit can also be computed, which sheds light on the character of phase space in the vicinity of the orbit. The continuation of families of periodic orbits generated by variations of any of the system's parameters, and the computation of the family orbits stability parameter helps then in understanding the dynamics of the problem.

The continuation of periodic orbits combined with the computation of stability diagrams is an old tool widely used in classical mechanics during the last three decades. In this sense, among a plethora of works, we refer the reader to Refs. 23 and 7 where two beautiful examples of the application of these techniques are shown.

A. Reduced problem

Because of the cylindrical symmetry of our problem, the study of the (ρ,z,P_ρ,P_z) phase space depending on the parameters (P_ϕ,δ,a) will provide enough information on the behavior of the system. Any desired solution will be completed by recovering the angular motion from Eq. (13).

As is well known, the linear stability of a periodic orbit is determined from the eigenvalues of the monodromy matrix. Since we are dealing with a Hamiltonian problem, the eigenvalues appear in reciprocal pairs, and as a consequence of the invariance of the equations of motion (12) we have one trivial eigenvalue $\lambda_0=1$ with multiplicity 2. Then, the stability index

$$k=\lambda+1/\lambda, \tag{17}$$

is normally used, where the condition k real and $|k|<2$ applies for linear stability, and the critical value $k=\pm 2$ means that a new family of periodic orbits has likely bifurcated from the original one. Therefore, stability diagrams where the stability index is presented versus the parameter generator of the family are commonly used.

Since we work with a reduced system of two degrees of freedom, the computation of Poincaré surfaces of section allows us to illustrate the phase space structure: In the regions of the phase space where the motion is regular, periodic orbits are clearly identified as fixed points of the surface of section.

Therefore, we proceed as follows: First, we identify the values of the parameters (δ,a) for which periodic analytical solutions exist in the phase space. Then, we carry out the numerical continuation of the families of periodic orbits—by varying one parameter, while the others remain constant—that give rise from those solutions. The stability diagram of every periodic orbit of each family as a function of the corresponding parameter is also computed. From this diagram, we can detect values of the parameter for which possible bifurcations take place. Bifurcations produce qualitative changes in the phase space structure. When a bifurcation is found, the study is completed by calculating the corresponding surfaces of section.

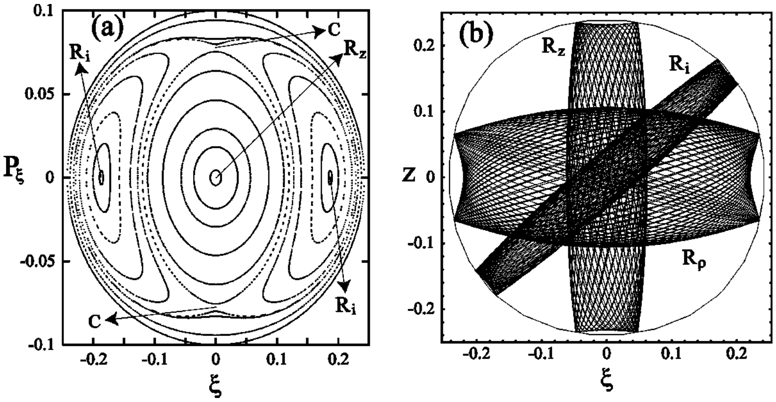

FIG. 3. (a) Poincaré surface of section ξ-P_ξ $(P_z=0)$. (b) Quasiperiodic orbits around R_i, R_z, and R_ξ. Both figures for $\delta=1/\sqrt{6}$, $a=0.2$, and $E=1/200$.

In searching for particular solution of Eq. (12), we find that rectilinear orbits along the ρ-axis $(z=0)$ exist always. Other particular solutions exist only for $P_\phi=0$:

- Rectilinear orbits along the z-axis $(\xi=0)$,
- rectilinear solutions with $z/\xi=\pm\sqrt{3/5}$, that exist for $\delta=\sqrt{1/6}$,
- circular solutions of radius $\xi^2+z^2=6E$, that exist for $\delta=\sqrt{1/6}$, and $a=0$.

1. The case $P_\phi=0$*: Variations of* δ

The special case $P_\phi=0$, where, again, we use ξ instead of ρ, was first considered in the Note.[8] We give here full details in this case, prior to consider the more general case $P_\phi\neq 0$.

To get a picture of the phase space where these four particular solutions exist, we compute the surface of section for $P_\phi=0$ and $\delta=\sqrt{1/6}$. For $P_\phi=0$, we define the surface of section as $P_z=0$ and $z\geqslant 0$. Under these conditions, it appears as a closed region in the plane (ξ,P_ξ) bounded by the curves

$$P_\xi=\pm\frac{1}{2}\sqrt{8E+(2\delta^2-1)\xi^2-6a\delta^2\xi^4}. \tag{18}$$

It is worth noting that the oscillations on the ξ-axis are tangent to the flux in this representation and they correspond to the curves (18).

Because we have to fix the energy E and the octupolar parameter a, we take $a=0.2$ and $E=1/200$. For $a=0.2$ the electrodes are quite deformed and this value is near to experimental real values.[18] On the other side, for $\delta=\sqrt{1/6}$, the energy $E=1/200$ is well below the energy E_S of the escape channels, which will be reached for

$$\delta^2=\frac{2}{7}-\frac{6a-\sqrt{3}\sqrt{125-80a+24a^2}}{35\sqrt{2}}, \tag{19}$$

that for $a=0.2$ gives $\delta\approx 0.786$. In the mentioned surface of section—see Fig. 3(a)—we distinguish four important structures:

(1) The stable (elliptic) fixed point located at (0,0) which corresponds to a rectilinear orbit along the z-axis. We name this fixed point and the corresponding periodic orbit as R_z. The levels around this orbit correspond to quasiperiodic trajectories with the same symmetry pattern; that is to say, mainly localized along the z-axis. In Fig. 3(b), named as R_z, is shown an example of this kind of periodic orbits.
(2) The elliptic fixed points symmetrically located at the ξ-axis correspond to the rectilinear orbits $z=\sqrt{3/5}\xi$ named R_i. The levels around these orbits correspond to quasiperiodic orbits mainly localized along $z=\pm\sqrt{3/5}\xi$—see orbit R_i in Fig. 3(b).
(3) The two unstable (hyperbolic) fixed points of the separatrix which divides the previous regions of motion. These hyperbolic points—named as C—correspond to almost circular orbits traveled in opposite directions which become circular of radius $\sqrt{6E}=\sqrt{3/100}$ for $a=0$.
(4) Finally, and taking into account that the limit of the surface of section is the rectilinear orbit along the ξ-axis, the levels above the separatrix correspond to quasiperiodic orbits mainly localized along this axis—see orbit R_ξ in Fig. 3(b). We name this fixed point and the corresponding periodic orbit as R_ξ.

Note that all the trajectories in Fig. 3(a) are connected by

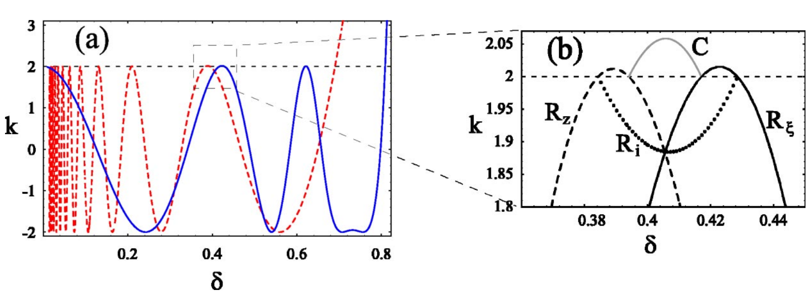

FIG. 4. (Color online). (a) Stability diagram of the family R_z of periodic oscillations on the z-axis (dashed line) and of the family R_ξ of periodic oscillations on the ξ-axis (full line). (b) Region of δ where the stable family R_i and the unstable family C exist.

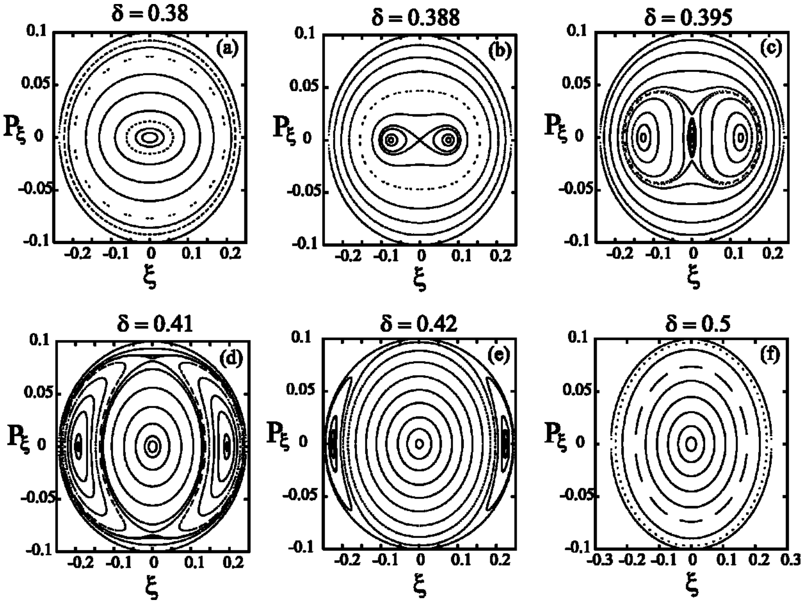

FIG. 5. Evolution of the surfaces of section ($P_z=0$, $z\geqslant 0$) for $E=1/200$, $a=0.2$ as a function of δ.

smooth lines. In this way, every trajectory seems to live on an adiabatic invariant torus. In conclusion, the system is (near) integrable at $E=1/200$. This is the expected result when the energy is much smaller than the escape energy E_S.

Therefore, we have available four periodic solutions to start the continuation procedure. We first compute the family of quasicircular periodic orbits that emanate from the circular solution from variations of the structural parameter a until reaching the value $a=0.2$ which will be considered fixed hereafter. Then, we study the variation of all four particular solutions as the control parameter δ varies. We call each family with the same name as the corresponding periodic orbit: R_ξ denotes the rectilinear periodic orbit along the ξ-axis as well as its family and so on with R_z, R_i, and C.

Variations of δ. First, we compute the families R_ξ and R_z. The stability diagram of these families is shown in Fig. 4(a).

Such a diagram gives the stability parameter k of each family as a function of δ. We see that family R_ξ—oscillations on the ξ-axis—shows a regular behavior ($|k|<2$) for $\delta<0.809$ and new bifurcations for $\delta\approx 0.242$, 0.423, 0.540, 0.623, 0.708, 0.756, and 0.809. The family R_z—oscillations on the z-axis—shows stability for $\delta<0.690\,296$ and new bifurcations for $\delta\approx 0.690$, 0.561, 0.390, 0.279, 0.210, 0.164, and 0.131. For smaller values of δ the stability behavior of R_z is highly oscillatory between the critical values ± 2 and with multiple bifurcations.

After a careful look to the values $\delta\approx 0.423$ and $\delta\approx 0.390$ given before, we see that not one, but two consecutive bifurcations are produced in their vicinity where the families R_i and C appear. As presented in Fig. 4(b), these families only exist in a narrow interval of δ. Thus, the periodic orbit R_i bifurcates first from the z-axis at $\delta\approx 0.385$ and immediately the periodic orbit C bifurcates at $\delta\approx 0.394$. Both families terminate on the ξ-axis: First the family C at $\delta\approx 0.417$, and then the R_i family at $\delta\approx 0.429$.

The described behavior is easily visualized by computing surfaces of section for some convenient values of δ ranging in the interval (0.38, 0.5). For $\delta=0.38$—see Fig. 5(a)—the surface of section presents only the stable fixed point R_z. The levels around this point correspond to quasiperiodic orbits mainly localized along the z-axis when they are near R_z, which become progressively quasiperiodic orbits along the ξ-axis as they go away from R_z; that is to say, as they approach to the limit of the surface of section. When $\delta=0.388$ a pitchfork bifurcation takes place: From the stable R_z—which becomes unstable—born the stable R_i orbits—see Fig. 5(b) for $\delta=0.395$. A second pitchfork bifurcation takes place when $\delta=0.394$ is reached: From R_z, which be-

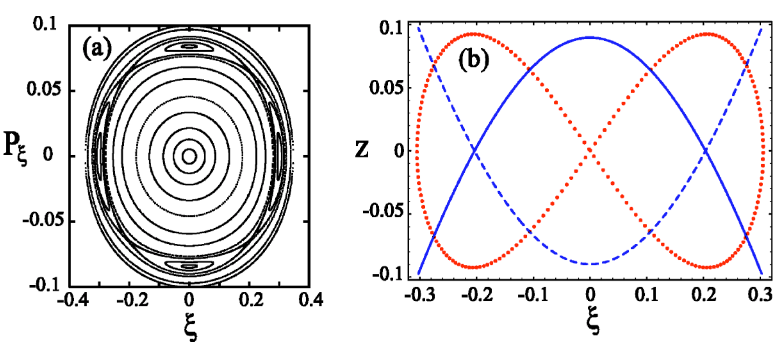

FIG. 6. (Color online). Left: Poincaré surface of section ($P_z=0$, $z\geqslant 0$) for $E=1/200$, $a=0.2$, and $\delta=0.6$. Right: ∪-, ∩-, and ∞-shaped orbits.

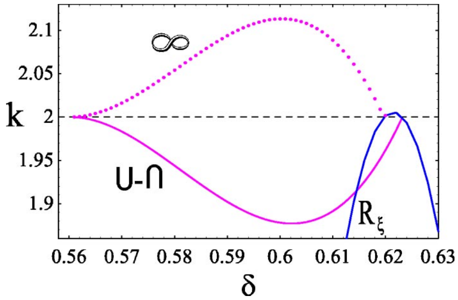

FIG. 7. (Color online). Families of stable ($|k|<2$) ∪- and ∩-shaped and unstable ($k>2$) ∞-shaped periodic orbits. All families bifurcate with period doubling from z-axis oscillations and end on ξ-axis oscillations with simple period.

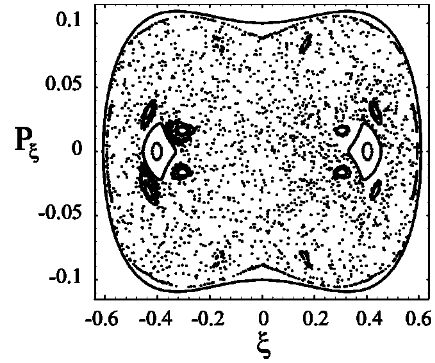

FIG. 9. Poincaré surface of section ξ-P_ξ ($P_z=0$) for $\delta=0.757$ and $P_\phi=0$

comes stable again, born the unstable C orbits—see Figs. 5(c) and 5(d) for $\delta=0.395$ and $\delta=0.41$. At this point, the phase space has the same structure as that we described in Fig. 3. A third pitchfork bifurcation takes place when the unstable periodic orbits C reach the limit of the surface of section for $\delta=0.417$, i.e., the periodic orbit R_ξ. From this bifurcation, only the orbit R_ξ survives becoming unstable—see Fig. 5(e) for $\delta=0.42$. A final pitchfork bifurcation occurs when orbits R_i reach the limit of the surface of section at $\delta=0.429$. As we can observe in Fig. 5(f) for $\delta=0.5$, the surface of section is made again of levels around R_z; a similar situation to that we found before the first bifurcation occurred.

According to Fig. 4, a very different behavior is found for $\delta>0.429$, where both C and R_i families disappear. Thus, in Fig. 6(a) we present a surface of section for $\delta=0.6$ where, besides the central elliptic point, we see four elliptic fixed points and four hyperbolic points corresponding to stable and unstable bifurcations of the axial trajectory for $\delta=0.5610$. The stable orbits are ∪- and ∩-shaped and the unstable ones are ∞-shaped traveled in opposite senses. Some examples of such orbits are depicted in Fig. 6(b). As appreciated in Fig. 7 both families terminate as oscillations in the ξ-axis with simple period, first the unstable ∞-shaped at $\delta=0.6196$, and then the stable ∪- and ∩-shaped at $\delta=0.6232$.

More bifurcations are produced for higher values of δ. Thus, in Fig. 8 we show a picture of the phase space for $\delta=0.7$, and several periodic trajectories. Thus, orbits (1, 2, 3) of Fig. 8 appear at $\delta=0.6229$ as stable—(1, 3)—and unstable—(2)—bifurcations of the z-axis oscillation with period triple. Stable (4, 6) and unstable (5) orbits bifurcate with four-fold period from the z-axis oscillation at $\delta=0.6500$. Unstable and stable orbits (7, 8) are eleven-fold bifurcations of the z-axis oscillation that occur at $\delta=0.6429$. The transition to instability of the z-oscillations takes place at $\delta=0.6903$ (cf. Fig. 4). Before this value all the solutions pass along the origin, but at this bifurcation, two almost vertical symmetric oscillations appear—orbit (9) in Fig. 8 and its symmetric with respect to the z-axis—that never pass through the origin.

For higher values $\delta>0.7$ the z-axis oscillation becomes highly unstable and the phase space is gradually filled with chaos. Figure 9 presents the case $\delta=0.757$ where chaos dominates the portrait alternating with chains of islands. In that figure we clearly identify the stable quasivertical oscillations at $\xi\approx\pm0.4$, and the two-fold stable orbits that surround them. These orbits appear at $\delta=0.7518$ as bifurcations of the quasivertical oscillations.

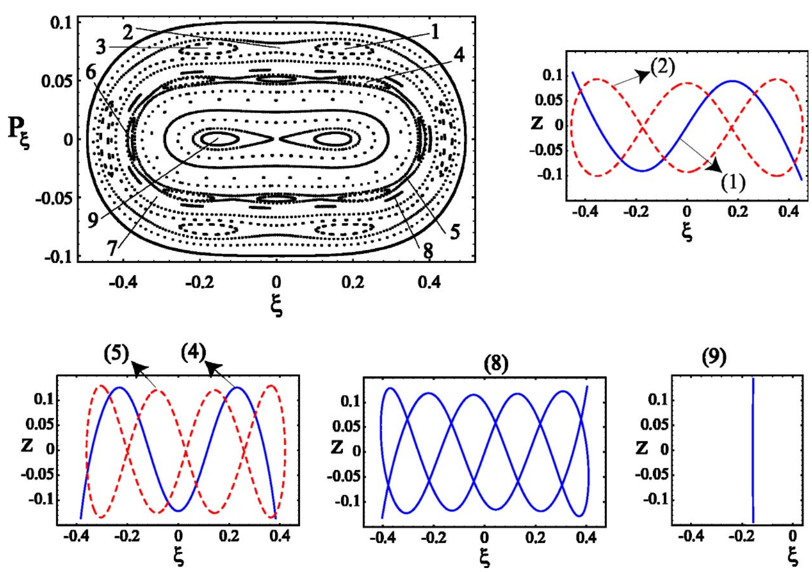

FIG. 8. (Color online). Above: Poincaré surface of section ξ-P_ξ ($P_z=0$) for $P_\phi=0$, $\delta=0.7$. Below: Several stable (1, 4, 8, 9) and unstable (2, 5) periodic orbits.

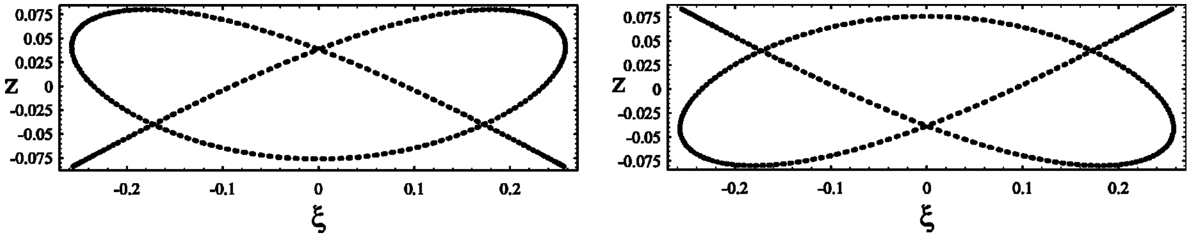

FIG. 10. Orbits of the families that start as four-fold period R_z orbits and end as three-fold period R_ξ orbits.

The three-fold periodic solutions (orbits 1, 2, and 3 of Fig. 8) are also found by visual inspection of Fig. 9 at, for instance, (0.176, 0.084). But most of the other periodic solutions have changed their stability character to instability and cannot be recognized in the figure.

A final comment is in order. Some orbits could be difficult to identify from visual inspection of the surfaces of section, even when they are stable. That is the case presented in Fig. 10, where two stable solutions—with stability index $k = 1.999\,992$ close to the limit value $k=2$—are presented ($a = 0.2$, $\delta = 0.5$, $E = 0.005$). Also, the bifurcations of the corresponding families are not appreciated in the stability diagrams, where only simple period and period doubling bifurcations can be appreciated. Each periodic orbit of Fig. 10 belongs to a family of periodic orbits that appears as a four-fold period bifurcation of the family of R_z orbits, and it exists only between $\delta = 0.468$, where it bifurcates from a R_z orbit, and $\delta = 0.506$, where it terminates as a R_ξ orbit. These kind of bifurcations with multiple period appear evident in the stability curves of the families of multiple-period periodic orbits, but its computation is time consuming.[10] On the contrary, it is known that for eigenvalues λ that are mth roots of the unity

$$\lambda = \cos 2\pi \frac{l}{m} + i \sin 2\pi \frac{l}{m},$$

where i is the imaginary unit and l and m are integer numbers, new families of periodic orbits may bifurcate from the original one. The resulting bifurcated orbit will be m-fold periodic (see, for instance, Ref. 11).

2. Variations of P_ϕ

In order to study the influence of the parameter P_ϕ in the dynamics of the reduced system, we start from the configuration given by $P_\phi = 0$, $\delta = 1/2$ and $E = 1/200$—see Fig. 5(f): the systems shows regular behavior and the phase space structure is determined by the presence of the two (stable) linear orbits R_z and R_ρ. From this configuration, we compute the families of periodic orbits for variations of P_ϕ.

Values $P_\phi \neq 0$ prevent the orbits from passing through the origin, in such a way that, while R_ρ orbits remain as oscillations on the ρ-axis, vertical oscillations R_z are forced to abandon the z-axis and are no longer rectilinear. Hence, R_z orbits are transformed to D-shaped trajectories that we call D_z orbits—see Fig. 11(b).

Figure 11(a) presents the evolution of the stability index k of the periodic orbits R_ρ and D_z as P_ϕ varies. As we can observe, orbits R_ρ are stable into the intervals $P_\phi \in [0, 0.02314]$ and $P_\phi \in [0.05598, 0.15357]$. For values $P_\phi > 0.15357$ the instability grows high. We note that these oscillations on the ρ-axis are periodic also with halved period because negative values of ρ are not possible in the case $P_\phi \neq 0$.

Stable oscillations D_z bifurcated from the z-axis start with almost vertical orbits and exist for $P_\phi < 0.0734\,66$—see Fig. 11(a). At this point the family comes back over itself with unstable orbits, until ending on the xy-plane for $P_\phi = 0.055\,98$.

Other trajectories appear as bifurcations of the family of R_ρ orbits. Besides the value $k=2$ corresponding to the termination of the unstable branch of D_z orbits at $P_\phi = 0.055\,98$, we find other values of P_ϕ for which $|k| = 2$ and new families of periodic orbits appear. Thus, for $P_\phi = 0.02314$ $k=2$, and a new family bifurcates from the family of R_ρ orbits. We name this family as the C_z family and its orbits as C_z orbits. In Fig. 12(a) we present the evolution of its stability index k. This new family starts with C-shaped orbits very close to R_ρ orbits. For increasing values of P_ϕ they apart from the ρ-axis until reaching a maximum value $z \approx 0.522$ for $P_\phi \approx 0.113$, and then they transform to

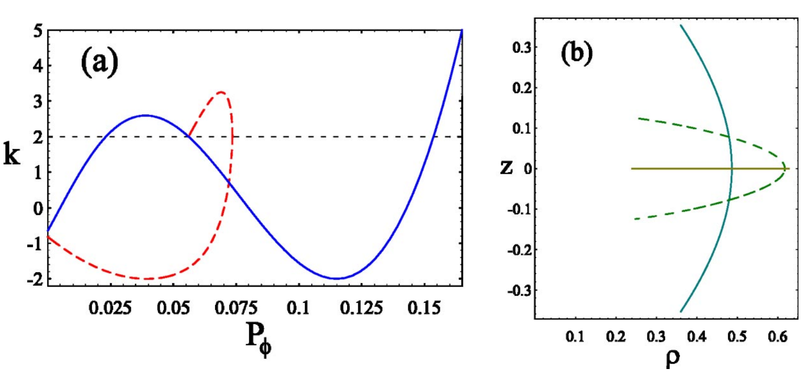

FIG. 11. (Color online). (a) Families of periodic orbits R_ρ and D_z for variations of P_ϕ ($E = 1/200, \delta = 0.5$) emanating, respectively, from the oscillations on the xy-plane (solid line) and from the z-axis (dashed line). (b) Three orbits periodic in the ρz-plane for $P_\phi = 0.06$. Two of them are stable and the other (dashed line) is unstable.

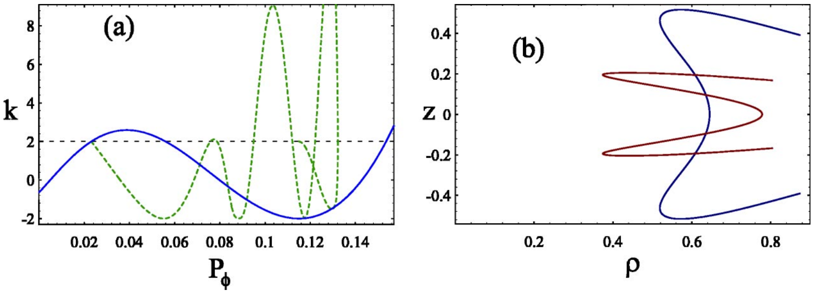

FIG. 12. (Color online). (a) Families of periodic orbits R_ρ and C_z for variations of P_ϕ ($E=1/200, \delta=0.5$). Note that the family C_z (dashed line) bifurcates from the family R_ρ (solid line). (b) Two stable Σ-periodic orbits for $P_\phi=0.121$.

Σ-shaped orbits—see Fig. 12(b). There is a maximum value $P_\phi=0.132\,21$ where the family comes back over itself until ending at $P_\phi=0.115\,00$, again as R_ρ orbit but with two-fold period. Finally, we can appreciate that the stability character of this family is oscillatory, passing several times from stability to instability with possible bifurcations.

The dynamical changes produced in the families of periodic orbits can be understood in terms of bifurcations of the fixed points appearing in the sequence of surfaces of section presented in Fig. 13. These surfaces of section, defined as $P_z=0$ and $z\geqslant 0$, are in the plane (ρ, P_ρ). Note that again, R_ρ orbits are tangent to the flux in this projection.

For $P_\phi=0.05$ (see surface of section I of Fig. 13), besides the two stable fixed points—the C_z (located at the right side) and D_z (located at the left side) orbits—some chaos appears in a region that closely surrounds the unstable R_ρ orbit. Also, we see the five-fold period bifurcation of the C_z family that is produced at $P_\phi=0.048$, and, as we stated before, that is not evident from the stability diagram of Fig. 12.

A period doubling bifurcation ($k=-2$) of the C_z family is produced at $P_\phi=0.055\,33$—see Fig. 12(a), and the corresponding bifurcation is appreciated in the surface of section II. Chains of islands in the border of the region of chaotic motion can be appreciated in pictures II and III. Also in picture III, a three-fold period bifurcation can be appreciated in the right side of the figure ($\rho\approx 0.6$); again, this bifurcation cannot be obtained from the stability diagram of Fig. 12.

Chaos disappears for $P_\phi\approx 0.07$, apparently in coincidence with the maximum instability of the D_z family, and only regular motion is appreciated in the surface of section number IV, where we also appreciate the hyperbolic fixed point ($\rho\approx 0.3$) corresponding to a D_z orbit of the unstable branch. The two branches of D_z orbits collapse at $P_\phi=0.0734\,66$ and the corresponding elliptic and hyperbolic fixed points disappear in an saddle-node bifurcation (see surface of section V). A new bifurcation of the C_z family takes place for $P_\phi=0.075\,82$, that is the pitchfork bifurcation that appears in the right side of surface of section V ($\rho\approx 0.66$). Chaos appears again close to this last value, and it gradually fills the surface of section for increasing values of P_ϕ (see picture VI).

Finally, one should note that, at a difference from the parameters a or δ, P_ϕ is an internal parameter that depends on the initial conditions of the ion.

B. Complete solution

Obviously, the R_z orbits are periodic in three-dimensional space. But the other orbits previously analyzed are only periodic in the ρz-plane, where

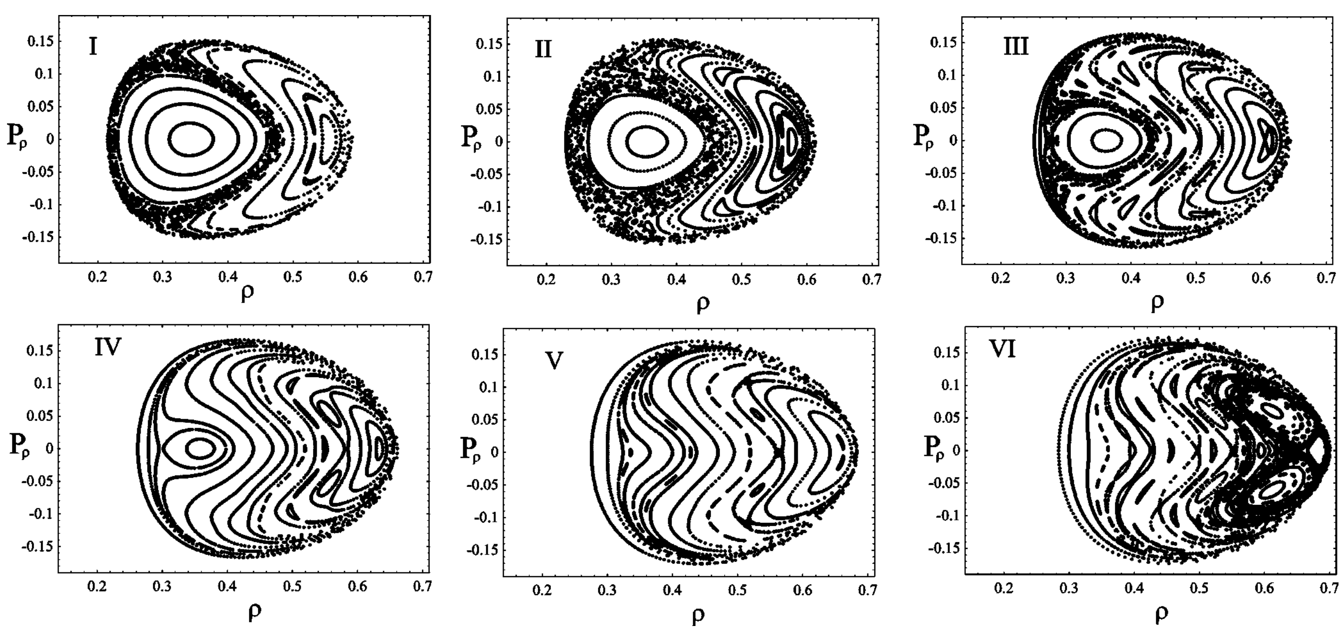

FIG. 13. Poincaré surfaces of section $\rho-P_\rho$ ($P_z=0, z>0$) for $E=1/200$, $\delta=0.5$ and, from left to right and from top to bottom, $P_\phi=0.05$, 0.056, 0.065, 0.07, 0.076, and 0.08.

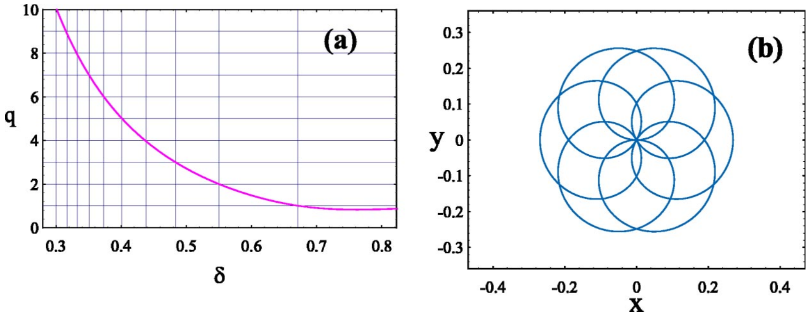

FIG. 14. (Color online). (a) Evolution of the commensurability condition q of the R_ξ family as a function of δ. (b) Three-dimensional periodic orbit R_ξ found for $q=3$ and $\delta=0.484$.

$$\rho(T)=\rho(0), \quad z(T)=z(0),$$

where, in general, $\phi(T)\neq\phi(0)$ conform Eq. (13), and they are not periodic in three-dimensional space. However when the difference $\Delta\phi=\phi(T)-\phi_0$ is commensurate to 2π the orbits are also periodic in the xy-plane and, consequently, in three-dimensional space. Therefore, we will find periodic solutions of the complete system by computing the ratio $q=\Delta\phi/(2\pi)$ for all the orbits of each family, which rational values m/n, with m and n integers, will point to periodic orbits in three-dimensional space after n periods. Several examples follow.

1. Family R_ξ ($P_\phi=0$)

Figure 14(a) presents a diagram with the evolution of the commensurability condition q along the family of R_ξ orbits for variations of δ. Rational values of q correspond to values of the parameter generator of the family, δ in this case, for which the orbits are periodic in the xy-plane. For instance in Fig. 14(b) we present a three-dimensional periodic orbit found for $q=3$ and $\delta=0.484$. Many other orbits periodic in the xy-plane could be obtained from other different ratios q.

2. Solutions for $P_\phi\neq 0$

In the same way, three-dimensional periodic orbits can be computed from any of the other families. Examples are presented in Fig. 15: One stable R_ρ orbit for $P_\phi=0.076$ (left), and an unstable (right) D_z orbit for $P_\phi=0.0634$.

V. SUMMARY AND CONCLUSIONS

In this paper we perform a systematic study of the periodic orbits and the evolution of the phase space structure of a single ion trapped in a realistic perturbed Penning trap. In particular, we introduce a quartic axially symmetric octupolar electrostatic perturbation that may be caused by imperfections in the experimental design. The advantage of managing this perturbation is that, despite its nonlinear nature, the system has only two degrees of freedom, which allows us to combine the numerical continuation of families of periodic orbits with Poincaré surfaces of section.

The Hamiltonian governing the dynamics of the system is stated and, after a convenient selection of units, the problem is seen to depend on the parameters a, P_ϕ, and δ. While the parameter a is related to the construction process of the trap, the parameters P_ϕ and δ can be externally established for a certain experimental process. Following the line of previous studies on quartic potentials,[22,23] in our study we keep constant the parameter a, while varying alternatively the two remaining, being the influence of P_ϕ in the Penning trap dynamics one of the main contributions of the paper.

The numerical study has been divided in three main parts. In the first part, by fixing $P_\phi=0$ and varying δ, we determined the stability diagrams for the fundamental families of periodic orbits. These diagrams indicate the presence of several bifurcations which are visualized by means of surfaces of section. In the second one, we carried out a similar study but now by fixing $\delta=1/2$ and varying P_ϕ. In these parts, the general effect of increasing the corresponding parameter is a pumping process through which periodic orbits emanate from two fundamental rectilinear periodic orbits: the vertical oscillation R_z and the ρ oscillation R_ρ. This process produces important changes (bifurcations) in the phase space structure. Finally, in the last part a gallery of exact periodic solutions in the three-dimensional space are shown.

We noted in the Introduction the crucial importance of periodic orbits in the understanding of the photoabsortion spectra on highly excited Rydberg atoms in external fields. In

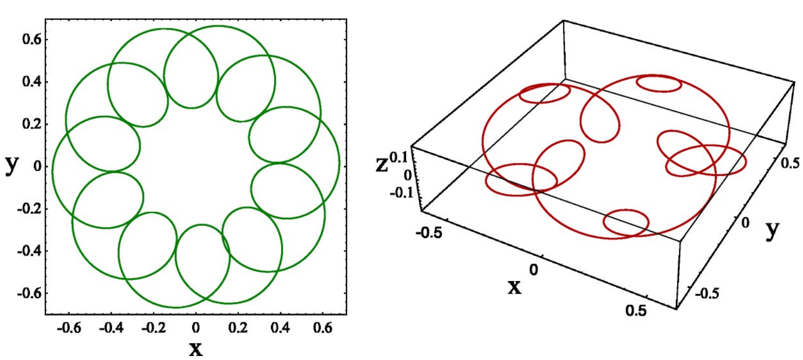

FIG. 15. (Color online). Two orbits of families R_ρ (left panel) and D_z (right panel) which are three-dimensional periodic orbits for different values of P_ϕ.

these systems, periodic orbits give important information about the absorption spectrum because each periodic orbit produces an oscillation in the spectrum and a peak in its Fourier transform. In this sense, the perturbed Penning trap presented in this paper could become an experimental opportunity to study the role played by periodic orbits in atomic systems. The experimental realization would consist of a Penning trap with electrodes having the appropriate octupolar deformation, which is controlled by the geometrical parameter a (see Fig. 1). As the perturbed trap is implemented, we can tune the external parameter δ (e.g., the strength of the external fields) to explore different phase space configurations. Moreover, the spectra should reflect not only the presence of periodic orbits but also the possible bifurcations between them because when a bifurcation takes place, the corresponding peak in the Fourier transformed spectrum becomes very large and then splits into two.[6]

ACKNOWLEDGMENTS

This work has been partially supported by Project No. BFM2002/03157 of Ministerio de Ciencia y Tecnología (Spain), Project No. ACPI2002/04 of Departamento de Educación y Cultura, Gobierno de La Rioja (Spain), and Project No. Resolution 92/2002 of Departamento de Educación y Cultura, Gobierno de Navarra (Spain).

[1] S. C. Farantos, Int. Rev. Phys. Chem. **15**, 345 (1996); M. Davis, J. Chem. Phys. **107**, 106 (1997).
[2] S. Keshavamurthy and G. Ezra, J. Chem. Phys. **107**, 156 (1997).
[3] M. C. Gutzwiller, *Chaos in Classical and Quantum Mechanics*, 1 IAM, (Springer-Verlag, New York, 1990).
[4] J. Main and G. Wunner, Phys. Rev. Lett. **82**, 3038 (1999).
[5] J. Main, G. Wiebusch, A. Holle, and K. H. Welge, Phys. Rev. Lett. **57**, 2789 (1986); A. Holle, G. Wiebusch, and K. H. Welge, Z. Phys. D: At., Mol. Clusters **6**, 295 (1987); G. Raithel, M. Fauth, and H. Walther, Phys. Rev. A **44**, 1898 (1991); A. D. Peters and J. B. Delos, *ibid.* **47**, 3020 (1993); **47**, 3036 (1993).
[6] J.-M. Mao, K. A. Rapelje, S. J. Blodgett-Ford, and J. B. Delos, Phys. Rev. A **48**, 2117 (1993).
[7] K. Efstathiou and G. Contopoulos, Chaos **11**, 327 (2001).
[8] M. Lara and J. P. Salas, Phys. Rev. E **67**, 027401 (2003).
[9] F. M. Penning, Physica (Amsterdam) **3**, 873 (1936); H. Dehmelt, Rev. Mod. Phys. **62**, 525 (1990).
[10] M. Lara, Celest. Mech. **86**, 143 (2003).
[11] I. A. Robin and V. V. Markellos, Celest. Mech. **21**, 395 (1980); E. Davoust and R. Broucke, Astron. Astrophys. **112**, 305 (1982).
[12] R. Blatt, P. Gill, and R. C. Thompsom, J. Mod. Opt. **39**, 139 (1992).
[13] J. N. Tan, J. J. Bollinger, B. Jelenkovic, and D. J. Wineland, Phys. Rev. Lett. **75**, 4198 (1995); T. B. Mitchell, J. J. Bollinger, D. H. E. Dubin, X.-P. Huang, W. M. Itano, and R. H. Baughman, Science **13**, 1290 (1998); W. M. Itano, J. J. Bollinger, J. N. Tan, B. Jelenkovi, X.-P. Huang, and D. J. Wineland, *ibid.* **30**, 686 (1998).
[14] S. L. Gilbert, J. J. Bollinger, and D. J. Wineland, Phys. Rev. Lett. **60**, 2022 (1988).
[15] J. I. Cirac and P. Zoller, Phys. Rev. Lett. **74**, 4091 (1995).
[16] R. Blatt, P. Gill, and R. C. Thompson, J. Mod. Opt. **39**, 193 (1992); R. C. Thompson, Comments At. Mol. Phys. **29**, 349 (1992); Adv. At., Mol., Opt. Phys. **31**, 63 (1993); G. Zs. K. Horvath, R. C. Thompson, and P. L. Knight, Contemp. Phys. **38**, 25 (1997); R. C. Thompson, Nathiagali Summer College, Pakistan, 1999.
[17] H. Walther, in *Irregular Atomic Systems and Quantum Chaos*, edited by J.-C. Gay (Gordon and Breach, New York, 1992); M. Moore and R. Blümel, Phys. Rev. A **48**, 3082 (1993); D. Farrelly and J. E. Howard, *ibid.* **49**, 1494 (1994).
[18] D. J. Bate, Ph.D. thesis, Imperial College, London, 1991; D. J. Bate, K. Dholakia, R. C. Thompson, and D. C. Wilson, J. Mod. Opt. **39**, 305 (1992).
[19] P. K. Ghost, *Ion Traps* (Oxford University Press, New York, 1995).
[20] M. Kretzschmar, Phys. Scr. **46**, 544 (1992).
[21] G. Zs. K. Horvath, J. L. Hernandez-Pozos, K. Dholakia, J. Rink, D. M. Segal, and R. C. Thompson, Phys. Rev. A **57**, 1944 (1998).
[22] P. Andrle, Bull. Astron. Inst. Czech. **30**, 285 (1979); N. Caranicolas and B. Barbanis, Astron. Astrophys. **114**, 360 (1982); E. Davoust, *ibid.* **12514**, 101 (1983).
[23] G. Contopoulos, H. Papadaki, and C. Polymilis, Celest. Mech. Dyn. Astron. **60**, 249 (1994).
[24] T. Bergeman, Bull. Am. Phys. Soc. **31**, 939 (1986); private communication; H. J. Metcalf and P. van der Straten, *Laser Cooling and Trapping* (Springer, New York, 1999).
[25] J. P. Salas, M. Iñarrea, and A. I. Pascual, Eur. Phys. J. D **20**, 45 (2002).
[26] E. Backhaus, J. Fajans, and J. Wurtele, Phys. Plasmas **6**, 19 (1999).
[27] T. M. Squires, P. Yesley, and G. Grabielse, Phys. Rev. Lett. **86**, 5266 (2001).
[28] J. D. Jackson, *Classical Electrodynamics* (Wiley, New York, 1975).
[29] H. Dehmelt, Am. J. Phys. **58**, 17 (1990).
[30] H. Friedrich and D. Wintgen, Phys. Rep. **183**, 37 (1989).
[31] J. P. Salas, A. Deprit, S. Ferrer, V. Lanchares, and J. Palacián, Phys. Lett. A **242**, 83 (1998).
[32] L. S. Brown and G. Gabrielse, Phys. Rev. A **25**, 2423 (1982); Rev. Mod. Phys. **58**, 233 (1986).